Experimental study concerning the interplay between gear ratio and field weakening for maximizing explosive motion of a jumping leg

J.M. Janbroers

***Abstract*—This work presents the experimental findings of a jumping leg setup to increment the jump height due to field weakening control. In total 60 experiments were executed and analyzed. The increment in height depends on the gear ratio of the setup and the field weakening algorithm. The highest increase in height is 10.8% with an increase of 56.9% in mechanical energy. The results show that field weakening can be used to increase the performance of an explosive motion.**

I. Introduction

A. Problem Statement

Robotic systems need to produce explosive motions in some situations. A jumping movement can be seen as an explosive motion in which a lot of torque and speed from the electric actuator is needed to perform the task. Unfortunately, a lot of torque at high speeds produced by the electric actuators might be unreachable due to system limits or physical limits. One of the constraints is the motor-controller-battery combination. When the rotor of an electric motor rotates, a voltage is generated by the motor. This voltage is called the back EMF. Due to the back EMF of the motor, the battery pack cannot produce enough voltage potential to produce enough current at high RPM. Available current 'degrades' at high rpm. Since the current is proportional to the torque, the available torque decreases at high RPM and therefore the rotational acceleration decreases resulting in presumable a lower jumping height compared to when this decrease in current does not occur.

Adding more powerful motors is not always the solution since powerful motors are often heavier. Increasing the total weight of the system with more powerful actuators can lead to the need for even hevier actuator, ending in a vicious cycle. Increasing the gear reduction is also not always an option since this can mean heavier gearboxes and less backdrivability of the actuator on impact which can lead to breaking end effectors. In [1], Wensing et al. stated that "Simply employing large motors to meet torque requirements is not viable in mobile robot design. Higher actuator masses contribute to GRF (ground reaction forces) requirements, and thus increase torque requirements. This relationship highlights the importance of maximizing torque density for actuators in legged machines. The power of the motor often becomes a major metric".

Changing the hardware of a robotic system has is drawback for improving the performance of explosive motions. Different motor control strategies can help to improve these explosive motions without adding weight to the system.

B. State of the Art

Research has been done to compose the highest jumping device. In [2] biological and engineered jumpers are analyzed and with this insight, a device was made that can jump over 30 meters high. This was done using a motor that can "multiply work". The design of this jumper uses a spring and an "highly geared"[2] electric motor to load this spring. The back EMF problem is not solved. Properties like the length and weight of different parts of jumpers are also discussed.

In [3] the problem of producing a high speed high torque with an actuator is discussed. A high-power-density variable transmission and a heat-dissipating structure are designed and tested. The gear ratio increases during acceleration. This proposed system was tested on different legged robotic systems. With this system, the highest jumping heights to date, for legged robots actuated with electric actuators, are obtained.

1) Fieldweakening in Robotics: Another way to make a robotic setup jump higher is to make the motors inside it, rotate faster. This can be done by controlling the permanent magnet synchronous machine (electric motor) in a non-conventional way. This is called field weakening. Field weakening counters the earlier mentioned back EMF.

The objective is not to control the motor to make more absolute torque resulting in more power, but to weaken the magnetic field at high rpm causing the back EMF to reduce. Because of this weakening of the magnetic field, the back EMF is lower at a high rotational velocity which results in a higher voltage potential between the voltage source and the motor. This higher potential difference causes less current degradation resulting in less torque degradation due to the lower back EMF compared to a non-field weakening application, resulting in a higher top speed with the same hardware.

There are two different field weakening control strategies. The difference between these two control strategies is the way the weakening of the field is controlled. This can be done by feedback control or feedforward control (model-based). Both methods have different modes depending on voltage and current limits. These modes enforce the current and voltage limits during field weakening operation.

2) Model Based Control: In [4], [5] and [6] a field weakening strategy is used where the current for the direct and quadrature direction are calculated by modeling of the electric motor. The values for these currents are obtained by predetermined formulas which consist of properties of the electric motor (like the resistance and inductance) and measurable

physical properties (like the current and rotational velocity of the motor).

The work of Rozendal et al. describes more than just a field wakening concept. [6] Describes the building and testing of a system that can jump. The field weakening concept is applied to make the system jump higher.

The work of Morimoto et al. in [4] also introduces the problem of demagnetization of the motor. Morimoto et al. states that 'magnet demagnetization due to the direct axis armature reaction must be prevented because the magnet torque decreases irreversibly if this demagnetization is very large.' Demagnetization due to field weakening is thus a drawback that can cause significant and permanent damage to the electric motor.

As stated by Rosendal et al. in [6] 'the model-based field weakening method is not without weaknesses. It is strongly dependent on the motor parameters.' The field weakening controller can generate different currents than intended because the system is modeled incorrectly. Furthermore, the motor parameters can change due to the ambient temperature changes but also due to operation. Rosendal et al. states that an increase of 50°C would increase the winding resistance by 20%. 3-phase PMSM can become over 50°C during operation. Furthermore the designing of a leg setup for a field weakening application was experienced difficult: "It turned out to be rather difficult to design a jumping leg that can accelerate fast enough for the motor to reach the field-weakening region." is stated in [6].

3) Feedback Control: Mohammadnia et al. proposes a feedback method. In [7] it is stated that the above-mentioned model-based approach relies on motor parameters '(...) which are subject to uncertainties, temperature variations and/or magnetic saturation'. Therefore a model-free field weakening approach is presented. In this paper, the model-based and model-free approach are compared. Despite the feedback approach being less sensitive to alternations of the motor parameters other problems were present. This approach was sensitive to noise resulting in the system not being able to keep the commanded voltage at the given limit [7].

4) Other Literature: The field weakening methods above are performed with surface-mounted permanent magnet synchronous motors. Another field weakening approach is chosen in [8] with interior-mounted permanent magnet synchronous motors.

C. Contributions

In this work, field weakening is proposed to boost the performance of a jumping leg setup without adding heavy actuators. This boost is done without using a different motor controller or changing operating limits. This proposed usage of field weakening should open the doors to incorporate field weakening control options in the design of the robotic setup so that better explosive performance can be designed with the same drive train (voltage supply, motor controller and electric motor). Only the gear ratio should be chosen carefully and an increase in torque and peak rotational velocity of the motor can be expected compared to a non-field weakening application.

This paper consists of the following sections: In section II the modeling of a permanent magnet synchronous motor is explained briefly followed by an explanation about field weakening. Section III discusses a computer model of a test setup and the design and realization of the physical test setup. Section IV discusses the results of the simulation of the test setup and discusses results and graphs from the tests performed by the test setup. Section V adds meaning to the results out of section IV. Section VI discusses the conclusion gained from the results. Recommendations about this research for future work is also discussed in section VI.

II. Analysis

A. Permanent Magnet Synchronous Motor

A permanent magnet synchronous motor (PMSM) can be described by a direct axis voltage and a quadrature axis voltage and the generated motor torque. According to Rozendal et al. in [6], the voltages can be described as

$$v_q = Ri_q + L_q\frac{di_q}{dt} + \omega_e L_d i_d + \omega_e \lambda_{pm}\,, \tag{1}$$

and

$$v_d = Ri_d + L_d\frac{di_d}{dt} - \omega_e L_d i_d\,, \tag{2}$$

and the torque for a surface PMSM can be described as

$$\tau_m = n\frac{3}{2}p\lambda_{pm}i_q\,, \tag{3}$$

where v_q and v_d are quadrature axis and direct axis voltages respectively. R is the phase resistance. i_q and i_d are respectively the quadrature axis and direct axis current. ω_e is the electrical angular velocity. L_q and L_d are respectively the quadrature axis and direct axis inductances. τ_m is the motor torque, n the gearbox ratio, p is the number of pole pairs of the motor and λ_{pm} is the permanent magnet flux linkage. Equations 1, 2 and 3 are obtained by the usage of the amplitude invariant Park and Clarke transformations. There are multiple types of transform which differentiate in for instance angle definition [9] or differentiate in power or amplitude invariant transformation [10] [9] [11].

according to [5] a setup of a motor and its power supply are limited by

$$i_q^2 + i_d^2 \leq i_{max}^2\,, \tag{4}$$

and

$$v_q^2 + v_d^2 \leq v_{max}^2\,, \tag{5}$$

with v_{max} being the maximum phase voltage.

The maximum rotational velocity of the motor is a function of the maximum phase voltage v_{max}, the number of pole pairs p and the permanent magnet flux linkage λ_{pm} [6] and can be described as

$$\omega_m^{max} = \frac{v_{max}}{p\lambda_{pm}}\,. \tag{6}$$

The maximum phase voltage is a function of the DC supply voltage v_{DC} [6] and can be derived as

$$v_{max} = v_{DC}/\sqrt{3}\,. \tag{7}$$

Equation 1 can also be drawn like an equivalent circuit. This circuit can be seen in figure 1. From the equation and from the figure, it can be seen that the voltage v_q increases proportional to ω_e due to the last term $\omega_e\lambda_m$ when the rotor rotates (set $i_d = 0$). This phenomenon, that a rotating PMSM generates voltage, is called back EMF. In figure 1b, two voltage sources are present: v_q and $\omega_e\lambda_m$. $\omega_e\lambda_m$ is referred to as the back EMF from now on.

Three phases of back EMF can be described as following:

- Phase 1 with $\omega_e = 0$: Equation 1 can be rewritten into

  $$v_q = Ri_q + L_q\frac{di_q}{dt}\,, \tag{8}$$

  with $i_d = 0$, $\omega_e = 0$ and $v_q \neq 0$. This results into a voltage difference in figure 1 between v_q and $\omega_e\lambda_m$: ($v_{diff} = v_q - \omega_e\lambda_m = v_q - 0$). Due to this voltage difference, a non-zero current is present: $i_q \neq 0$. Therefore torque is created according to equation 3.
- Phase 2 with $\omega_e \neq 0$: When the rotor speeds up due to the motor torque, $\omega_e\lambda_m$ increases with ω_e. The equation describing v_q with $\omega_e \neq 0$ and $i_d = 0$, is derived from equation 1 and is described as

  $$v_q = Ri_q + L_q\frac{di_q}{dt} + \omega_e\lambda_m\,. \tag{9}$$

  The potential difference between the two voltage sources in figure 1B is now: ($v_{diff} = v_q - \omega_e\lambda_m$). Because of the lower voltage difference due to the back EMF, current i_q is smaller than before resulting in less torque than before according to equation 3. This means that the rotor will accelerate less when the angular velocity increases.
- Phase 3 with $\omega_e >> 0$: When the rotor speeds up more, the voltage difference between the external voltage source and the back EMF ($\omega_e\lambda_m$), can become zero ($v_{diff} = v_q - \omega_e\lambda_m$ = 0). When this happens, the current i_q also approaches zero. This results in zero motor torque according to equation 3. Zero motor torque means no acceleration of the rotor. The angular velocity will not increase anymore.

  When performing an explosive motion, the back EMF and the effect it can have on the quadrature axis current can limit the explosive motion of a PMSM, especially when the maximum available and rated voltage is applied to the terminal (maximum so that the voltage produced by the external voltage source cannot be increased). This results in less applied torque and thus less acceleration.

B. Motor Controller

A motor controller can control the above-mentioned quadrature current i_q by applying a voltage to v_q in figure 1. The motor controller thus controls the motor torque by controlling the current via applying a voltage over the phases of the PMSM. A motor controller cannot produce unlimited voltage. The motor controller is dependent on the power supply. The maximum phase voltage it can produce is a function of the DC supply voltage described in equation 7. when the motor accelerates and when the motor controller applies the maximum phase voltage, it cannot produce more phase voltage to counter the back EMF to maintain a certain current/torque command. Then phase 2 and phase 3, described in section II, occur.

C. Field Weakening

To counter the decreasing acceleration and torque due to the back EMF discussed above, the current in the direct axis can be used. The direct current during normal control of a PMSM in normal operation is set to zero, $i_d = 0$. This current can be used to weaken the magnetic field by making a magnetic field in the opposite direction of the magnets on the rotor. This is called field weakening. Due to field weakening, the back EMF can be reduced, and thus higher rotational velocity can be reached.

In figure 1B and in equation 1 the result of a non-zero direct current $i_d \neq 0$ can be seen creating another voltage source "$\omega_e L_d i_d$" countering the Back Emf "$\omega_e\lambda_m$".

Multiple variations of how to apply field weakening exist. There is for example feedback fieldweakening described in [7] which uses feedback. In this paper, the model-based concept by Roozing et al in [5] is discussed and applied.

1) Model Based Control: Fieldweakening by sending current through the direct axis ($i_d \neq 0$), does not contribute to more torque directly since i_d is not present in equation 3. When only a limited amount of current is available, a decision has to be made about how much current needs to be applied in the direct axis or in the quadrature axis. In [5] an algorithm is proposed which calculates the wanted current values in the direct and the quadrature axis. This algorithm is model-based, meaning that the algorithm uses predetermined motor parameters, their power supply parameters and the wanted torque reference to calculate the suitable direct and quadrature currents. The rotational velocity is the only feedback signal needed for this algorithm to work. The motor-power supply conditions from equations 4 and 5 are also met in this algorithm.

The decision on how much current to apply to the direct and quadrature current depends on which mode the motor is operating in. In figure 2 the different modes can be seen with different quadrature and direct currents for an accelerating PMSM. The red circle represents the maximum allowable current for the whole system due to for instance the maximum rated current for the motor controller. The first mode of the algorithm when a PMSM is accelerated is mode 0. Mode 0 in this figure represents the phase when enough current is available to apply the commanded quadrature current. Mode 1 occurs when less current is available in the quadrature direction than the commanded quadrature current due to the increasing back emf. Direct current is then used to counter the back EMF. The direct current can be applied without having to reduce the quadrature current since mode 1 is within the red circle. The back EMF will increase more when the motor speeds up more and more direct current will be added until

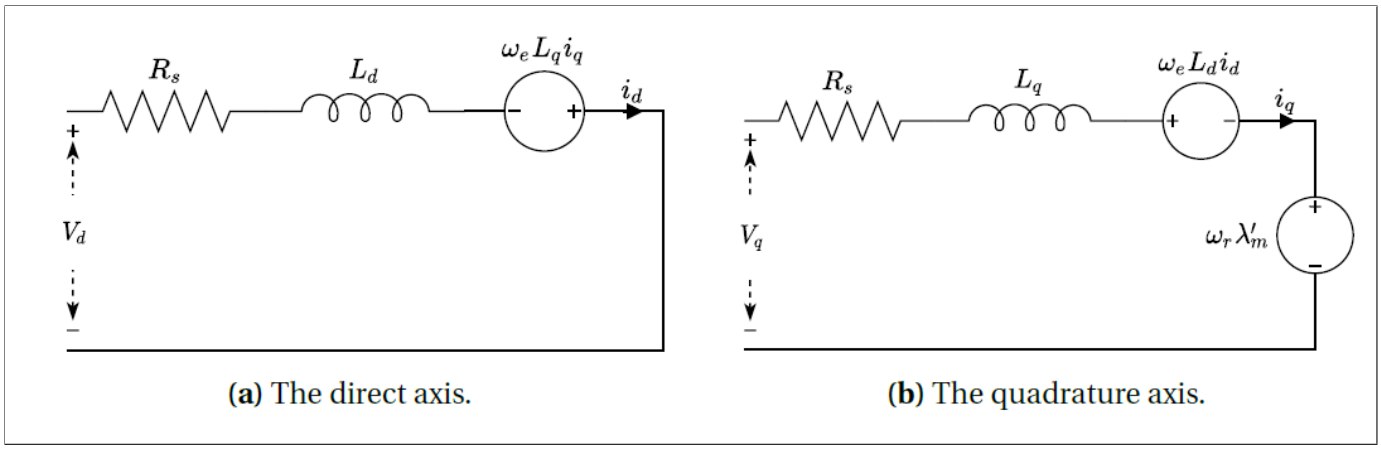

(a) The direct axis. **(b)** The quadrature axis.

Fig. 1: Equivalent circuits of the quadrature and direct axis [6].

mode 1 reaches the red circle. In point C mode 2 is entered and the quadrature current needs to be lower to allocate current to not exceed the current limit and to allocate current to the direct axis. Torque will be reduced by the reduced quadrature current but more torque will be present compared to a non-field weakening situation. mode 3 is entered when the motor is being driven externally. This mode is outside the scope of this work

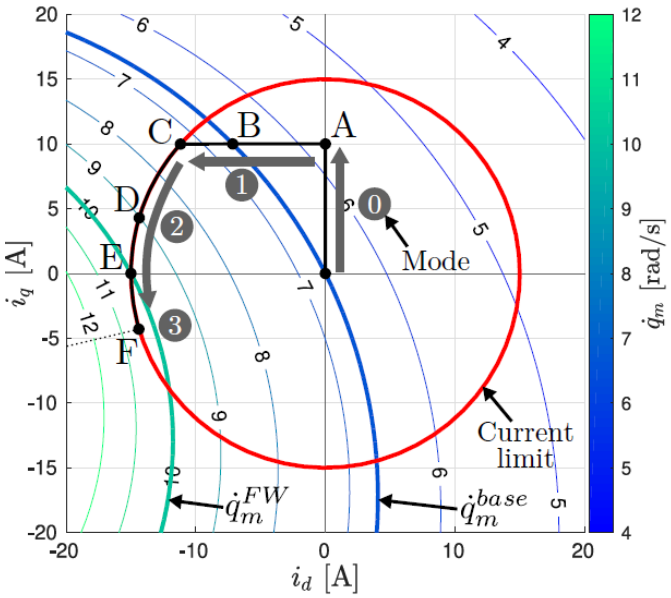

Fig. 2: i_d & i_q diagram of field weakening modes [5].

A model-based algorithm uses pre-determined parameters of the motor and the motor controller. These predetermined parameters differ due to for instance heat or human error when determining the value. When the parameters cannot be determined, estimates have to be made in order to make the algorithm work. Different and/or less accurate output can be obtained by the algorithm due to these parameter estimations and differences. A feedback method compared to the model-based method, does not have this weakness since it only uses feedback to determine the right current commands. A feedback signal does contain noise meaning that a feedback method can produce unreliable and less accurate output when noise is present in the system.

2) Operating Range: The operation range of field weakening is important to effectively use field weakening. Direct current is only applied by the model-based algorithm when the back EMF is reducing the commanded quadrature current (mode 1 and 2 in figure 2. This is from now on referred to as the field weakening operating range. In this range v_{diff} in $v_{diff} = v_q - \omega_e \lambda_m$ becomes lower than needed to produce the commanded quadrature current. Direct axis current does not contribute to the amount of torque according to equation 3 meaning that the direct axis current is useless outside of the field weakening range. Using field weakening outside of the field weakening operating range causes the direct current to contribute to more heating of the motor.

This field weakening operating range can be tuned via a gearing ratio since the back EMF ($\omega_e \lambda_m$) is a function of the rotational velocity. With a gearing ratio, the torque applied to a load (after the gearbox) can be changed meaning that the acceleration time is altered and the top speed of the load can be changed. This changing of the load torque and acceleration changes the motor acceleration and thus the time to accelerate to the field weakening operating range. The trade-off between acceleration and maximum rotational velocity can be seen in figure 3. Choosing the gear ratio is thus a balancing act between the reachable maximum velocity and the time to accelerate to this velocity. When a gearing ratio is too low, the maximum velocity is reached too early but the system could have accelerated longer to a higher maximum velocity. When the gearing ratio is too high, a lower maximum velocity is reached since the acceleration is too low. The theoretical maximum velocity is then never reached.

The gear ratio determines the velocity where the torque decreases due to the back EMF and thus when field weakening is activated. The gearing ratio, and thus the torque versus the rotational velocity profile, determines the performance of an explosive motion.

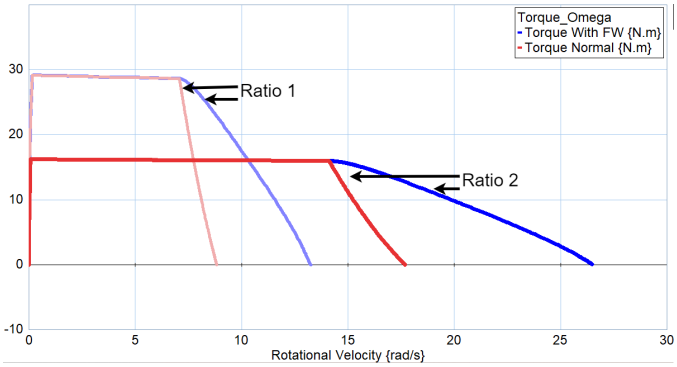

Fig. 3: Torque plotted versus the rotational velocity of a system with a PMSM and two gearboxes with arbitrary values. The red lines represent the torque plotted versus the rotational velocity without field weakening and the blue lines represent the torque versus the rotational velocity with field weakening. The bright red and blue lines are plotted with a twice as big secondary gearing ratio than the light red and blue lines.

III. Design and Realization

In order to see if field weakening can be used in a robotic setup for an explosive motion, a test setup is created to mimic a robotic setup based on the design by Rozendal et al. in [6]. The design of the jumping leg setup seen in 4 was chosen since it consists of a leg and cannot fall over during jumping. This setup can jump in a vertical direction. A rigid frame is created and due to the two poles and linear bearings, only vertical motion is allowed for the main body of the robot while minimizing friction. The foot in the leg is also connected to one of these vertical poles with a linear bearing in order to allow vertical motion for the foot too. A lot of control which is needed to make a robotic setup stand on its own, is now not needed due to the movement restrictions. Therefore only a simple motor can be fitted to the main body to accelerate the upper leg via gears to extend the leg. This way control is only needed to accelerate and decelerate the motor resulting in the main body moving up and down along the poles.

A. System architecture

The system architecture of the new design can be seen in figure 5. The motor controller (Odrive version 3.6) is directly controlled by the microcontroller (Pi Pico) via UART. The microcontroller sends current, position or other commands or data requests to the motor controller. The microcontroller can receive signals (logic high or logic low) from the control panel. The motor controller can also write saved data to the laptop via UART. The pi pico is programmed with the Arduino IDE.

The motor controller executes the commands from the microcontroller by applying the correct voltage over the phases of the PMSM. When feedback is demanded, it transmits Velocity (turns/sec), position (turns), direct current value and quadrature current value via UART to the microcontroller.

Storage on the microcontroller is used to store this data and this data is only sent to the laptop until the command has been executed in order to leave all the computational power to the execution of the command.

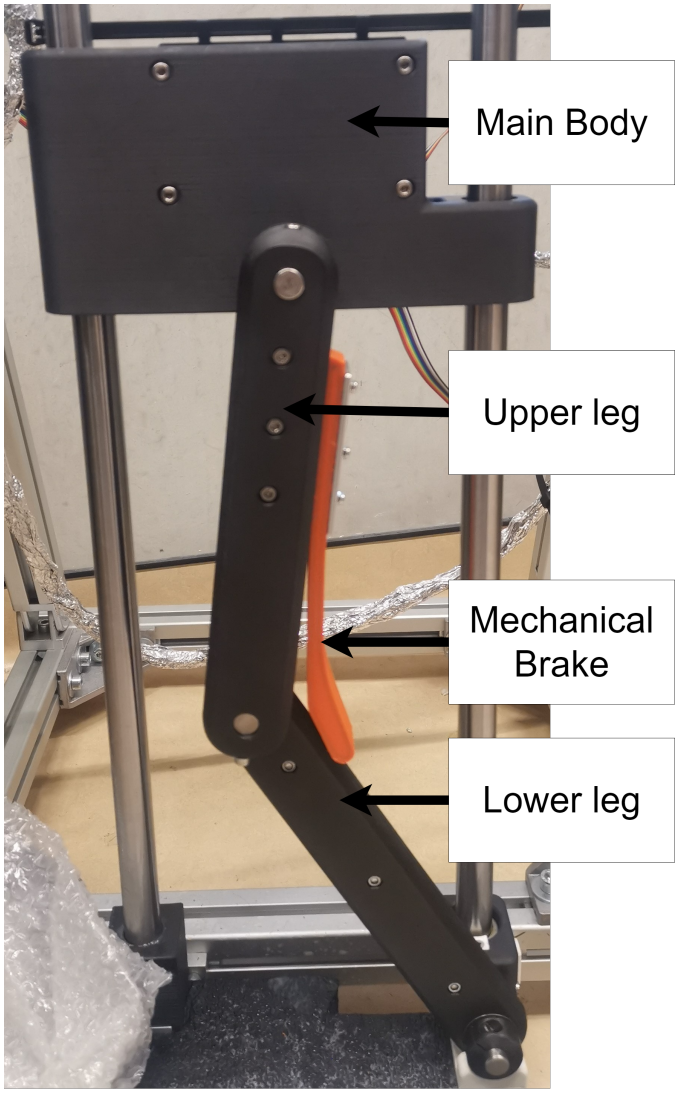

Fig. 4: Jumping leg setup constrained by the vertical gliding poles.

1) Micro Controller: This system architecture was chosen in order to have a dedicated microcontroller instead of a personal computer since this increases the mobility of the setup. The Pi Pico can also be overclocked when needed. This can be useful for exploring the effect of clock frequency on field weakening operations. The Pi Pico also has enough RAM available to store all the collected data until the execution of a program is done. This data is sent to the laptop after the execution of the program. Due to the data logging and sending afterward, the programs are executed without any interrupts from the data sending. This results in a faster calculating rate for the model-based algorithm.

2) Control Panel: The control panel is designed to easily control the setup via push buttons. The control panel is built from push buttons, pull-down resistors, protoboard and printed parts out of though PLA filament.

3) Laptop: The laptop is only used to store data. This data is stored via a Matlab program.

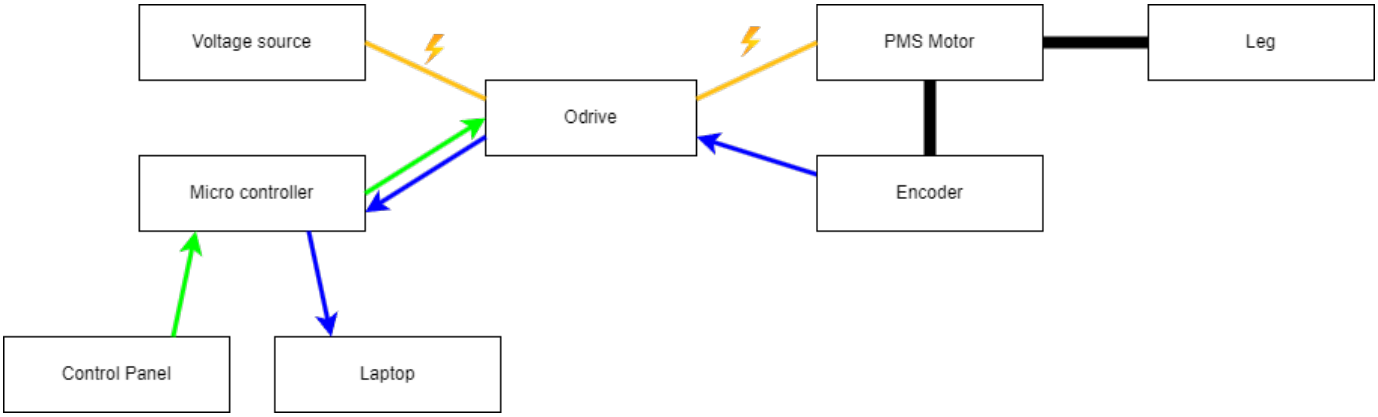

Fig. 5: Schematic representation of the setup within green command signals. In blue feedback signals. In yellow power cables and in black physical connections.

B. Mechanical System

The physical part of the jumping robot consists of the PMSM with gearbox, encoder and the jumping leg.

1) Motor and Gearbox: The motor chosen for this design is the 614949 Maxon EC 60 flat 60mm brushless 200-watt motor. This Motor has a "Maxon encoder MILE 512-4096 CPT" encoder and a 223089 "maxon Planetary Gearhead GP 52C 52mm". This motor configuration has also been used in [6]. This motor configuration was chosen since this configuration was already present. The planetary gearhead has a reduction of 43 meaning that the rotational speed of the motor is reduced to 1/43th after the gearhead and the torque is increased 43 times.

2) Gearing Ratios: After the 43 reduction, a gear multiplication is needed in order to let the leg produce enough velocity to jump off the ground [6]. As mentioned in sections I-B2 and II-C2, it is important to reach the Field weakening operating region. Only then a jump with and without field weakening can be compared. To make sure that this region can be reached, multiple secondary gears are designed. In order to get into the field weakening region more than Rozendal et al. in [6], the secondary gearing should be lower than the gearing ratio in [6]. Rozendal et al. used a secondary ratio of 2. A ratio that is too low causes a lot of torque and high acceleration but a reduction in maximum rotational velocity. This means that the perfect ratio should be found which brings the setup in the field weakening region during acceleration but does not result in a too-low velocity of the leg. This is done by creating 5 different secondary gearing ratios. 3 ratios will be lower than 2. One ratio will be the same as 2 and one ratio will be above 2. The ratio of 2 and 2.3 is chosen as a control group to see if the assumption to have a ratio below 2 increases the field weakening region. In table I, the maximum torque and maximum velocity without field weakening operation are presented. The gears were printed via a Mark Forged metal X out of "17-4 PH Stainless Steel" filament.

3) 3D Printing Leg and Motor Mount: The leg created by Rozendal et all. in [6] was 3D printed in PLA and Though PLA. Unfortunately, these parts started showing cracks. These cracks started to occur when jumping with the setup. In order to prevent a catastrophic failure, these parts are printed with other materials. The legs are printed by the Markforged Mark 2 out of the "Markforged Onyx-Filament FFF" and the "Markforged Carbon Fiber CFF Filament". The main body, where the motor and the leg is attached to, is printed by the Bambu Lab X1-Carbon printer out of "Prusament PC Blend Carbon Fiber Black".

ratio	torque (Nm)	maximum motor velocity (rad/sec)
1	34	4.0
1.3	26	5.3
1.6	21	6.5
2	16	8.2
2.3	14	9.4

TABLE I: Secondary gearing ratios with the expected torque (for $i_q = 15A$) after the secondary gearing ratio and expected maximum velocity after the secondary gearing ratio calculated with equations 3, 6 and 7.

Play between the shaft of the first gearbox and the metal printed gears due to damage to the key seat of the first gearbox, was a reason for concern. This play means that there are multiple leg positions possible for a commanded motor position. This play can also cause unwanted effects during the transition from accelerating to decelerating the leg during the execution of a jump. This play is difficult to get rid of since the keyway of the first gearbox was damaged. Therefore a mechanical brake/ spring was created to make sure that the play could not cause problems during decelerating the leg mid-air and causing the setup to land in an unintended way. This mechanical brake is printed by the anisoprint printer out of "Anisoprint CCF (Composite Carbon Fiber)". The leg and mechanical brake can be seen in figure 4. The play should not cause any trouble during acceleration since the motor forces the key in the damaged key seat to one side due to the acceleration and therefore during acceleration, the play is gone.

C. Field Weakening Algorithms

To see if field weakening can help the performance of explosive motions for robotics setup, 4 different algorithms are programmed. These Algorithms should be performed with all 5 gearing ratios presented in table I. the setup should be brought

into the squatting position and the fully extended position and marked via the control panel.

1) Normal Jump: A normal jump is programmed in which field weakening is deactivated. This is the base test. The motor accelerates from the squatting position to the extended position. The leg is now airborne. The motor controller goes into a position control loop and forces the fully extended position after acceleration. The leg lands in the fully extended position to minimize torque on the gearboxes. The maximum current is set to 15A to not exceed the rated continuous output torque for too long and remain under the "intermittent" gearbox torque of the Maxon gearbox.

2) FW Version 1: Field weakening version 1 is the same as the "normal jump" but field weakening is activated. This test is designed to see the difference with the Nomral Jump and the original field weakening algorithm.

3) FW Version 2: Field weakening version 2 is the same test as the "FW version 1" but the DC voltage value in the algorithm by [5] is altered a bit. Due to losses in the cables, the DC voltage at the motor controller might be lower than at the power supply. The same holds for the voltage delivered by the motor controller and the voltage present at the motor. These losses are compensated by altering the DC voltage value in the algorithm code. Current dips, when the measured current does not reach its commanded current, can occur when the algorithm works with a slightly incorrect value for the DC voltage value. The current dips should be less or non-existent due to this compensation.

4) FW Version 3: Field weakening version 3 is the same test as the "FW version 2" but the maximum current is altered. The maximum current in the quadrature direction is set for 15A maximum but the total maximum current is set for 30A max. This means that the field weakening algorithm can now allocate current to the direct axis if needed without having to reduce the quadrature current immediately which is the case for FW version 1 and 2 since the total maximum current is set for 15A in those tests due to the gearbox restrictions. The direct axis current is only limited by the temperature of the motor controller and the motor and not limited by the gearbox since no torque is produced by the direct axis current. This thermal restraint is not applicable during these short explosive jumps when enough time between jumps is allocated.

IV. Experimental Results

3 attempts were made of the 4 different algorithms mentioned in section III-C per gear ratio mentioned in table I. In total sixty jumps were executed. The jump height of each jump was recorded with a camera at 120 frames per second. These recordings were analyzed by eye and written down. With height, the distance between the top part of the body and the test-setup ground is meant. The heights were rounded to the closest 0.25 cm value due to the resolution of the camera. All other measurements shown in this section are captured by the Pi Pico with a sample rate between 4 to 7 milliseconds and sent to the laptop after a complete jump. The errors during these tests are described in the appendix.

A. Jumping performance

In figure 6 the average height per gearing ratio and test can be seen. The highest average height is obtained by a gearing ratio of 1.3 with FW V3. In figure 7 the height increase compared to the normal jump, averaged over 3 attempts can be seen. The heights of gearing ratio 1.6 and 1.3 increase 3.8% 10.5% respectively, going from normal jump mode to field weakening version 3. Ratios 2 and 2.3 decrease by 2% and 1.7% respectively. The reached height for ratio 1 is the lowest of all the gear ratios.

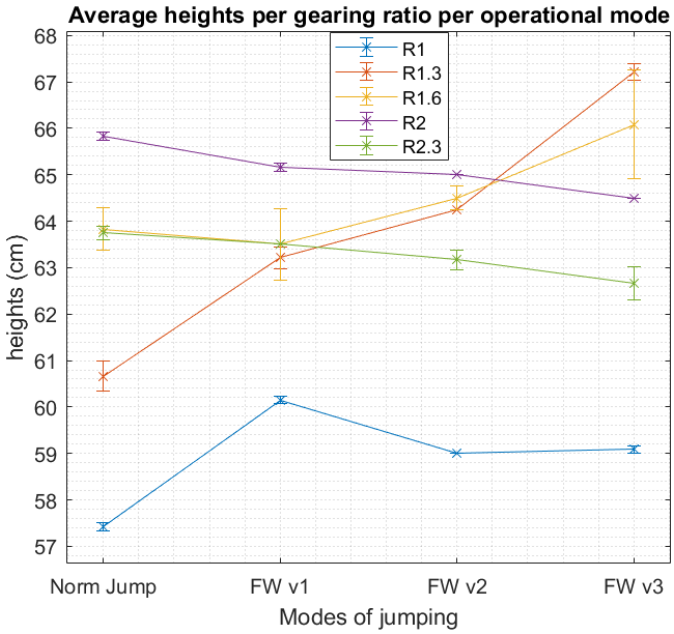

Fig. 6: Jump height averaged over 3 attempts each for every gearing ratio.

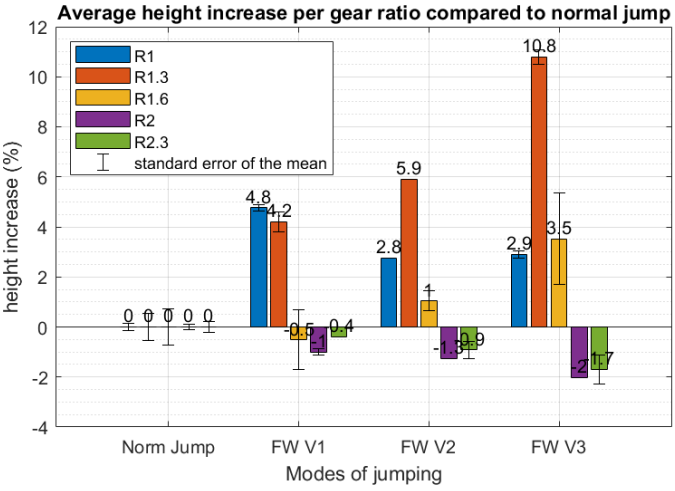

Fig. 7: Height percentage averaged over 3 attempts each for every gearing ratio .

In figure 8 The leg velocity versus the leg position is plotted for the different field weakening modes per ratio for attempt 1. Only Attempt 1 is plotted since the other attempts show similar results. In these plots, the trajectory of the leg starts at an angle of 28°in the squatting position and stops at 172°in the fully

extended position. For ratios 2.3 and 2 the four different jump types are plotted on top of each other. The phase plots of ratios 1, 1.3 and 1.6 show a clear variation in rotational velocity. For all three ratios, the Norm Jump has the lowest rotational velocity. After Norm jump, FW V1 has more velocity during the movement, FW V2 comes after that and FW V3 has the highest velocity for ratios 1.6 and 1.3. This order is not present for ratio R1.

B. Energy injection

In figure 9 the amount of mechanical energy produced by the motor is displayed as a percentage of the energy used by the normal jump mode per gearing ratio. The mechanical energy was obtained by integrating the mechanical power produced by the motor. The three attempts are averaged per ratio and test mode. For ratios 1, 1.3 and 1.6 an increase of the energy can be seen during acceleration of respectively 85.8%, 56.9% and 27.9% with field weakening version 3. For ratios 2 and 2.3 a slight increase can be seen of respectively 5.5% and 0.4% in field weakening version 3 mode. The total averaged energy per ratio and per test mode can be seen in figure 10 . The total energy of ratio 1 during all field weakening versions is higher than the total energy of all the other ratios during all field weakening versions.

In figure 11 the current in the quadrature and direct axis can be seen for the different field weakening modes per ratio for attempt 1. Only Attempt 1 is plotted since the other attempts show similar results. For ratio 1, a clear distinction between the different field weakening modes is visible. The blue line is near zero in the D current axis. FW mode V1 and V2 goes toward the green circle and stay on the inner green circle representing a declined quadrature current but an increased direct current as expected by field weakening. FW V1 and V2 differ only in the way they reach the green circle. The path of FW V1 to the green circle has a lower quadrature current than FW V2. The DC voltage compensated FW V2 version does not follow the green circle perfectly and also first decreases in the quadrature direction but FW V2 dips less than FW V1. FW V3 is lower than the dark blue line representing the quadrature maximum current of 15A before it reaches and follows the green line.

For ratios 1.3 and 1.6 the same is true as described above but the lines are a bit more scattered. FW V1 does in both cases not reach the inner green circle (except when the direct current is zero).

For ratios 2 and 2.3, FW V1, V2 and V3 do not reach the green circles except when the direct current is zero. FW V1, V2 and V3 are almost plotted on top of each other for the ratio of 2.3

In figure 12 the amount of samples taken during field weakening operation during acceleration is represented in a percentage of the total amount of samples during acceleration. This acceleration is the movement of the leg from a squatting position to the fully extended leg. For all the ratios an increase in field weakening samples is present.

V. Discussion

In table II the percentage gains of field weakening version 3 from figure 7,9 and 12 are displayed next to each other.

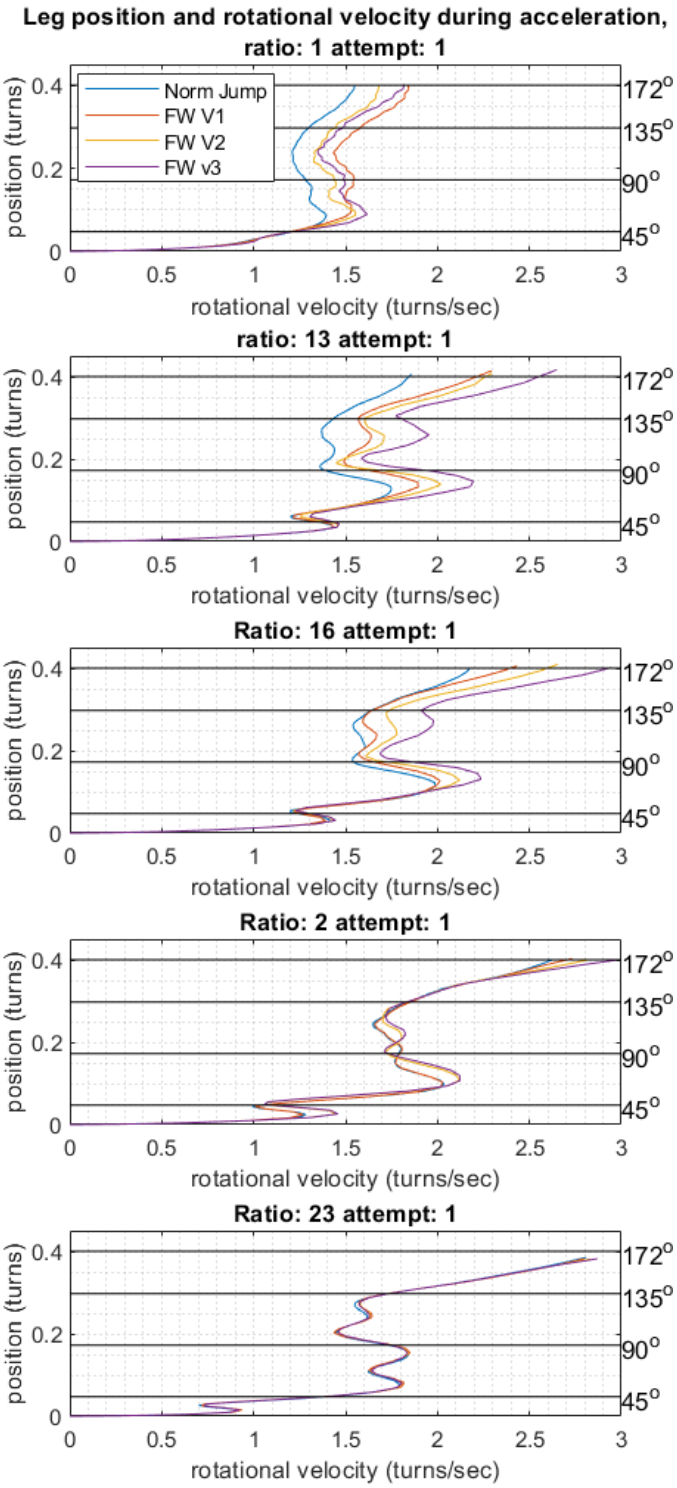

Fig. 8: Position of the leg plotted versus the velocity of the leg in respectively turns and turns per second. Only attempt 1 for the 4 different jump modes and for the different ratios is shown.

Also, the ratio between the energy increase and height increase (energy increase of FW V3 divided by the height increase of FW V3) per ratio, is presented.

From this table, it can be seen that there is a small height decrease for ratios 2 and 2.3. This while there is only a small (relative to the other ratios) increase in energy, respectively

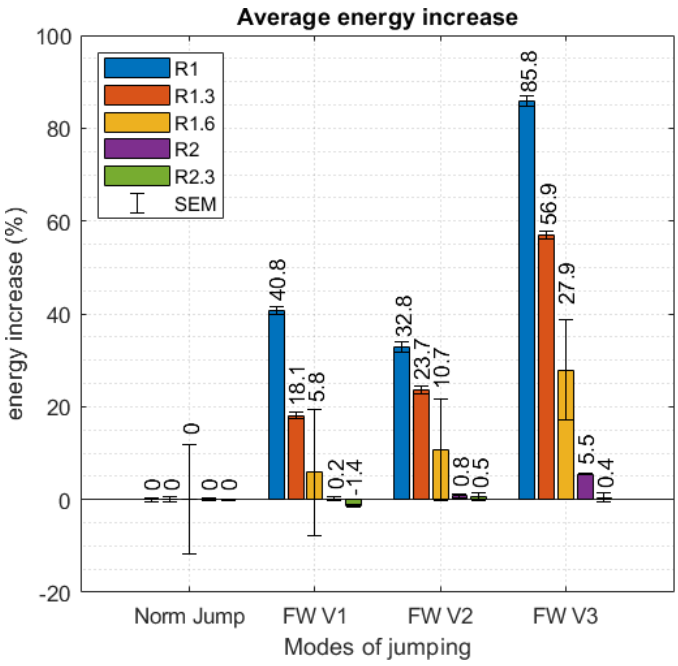

Fig. 9: The mechanical energy produced by the motor displayed as a percentage increase relative to a normal jump during acceleration per ratio, per jump averaged over 3 attempts.

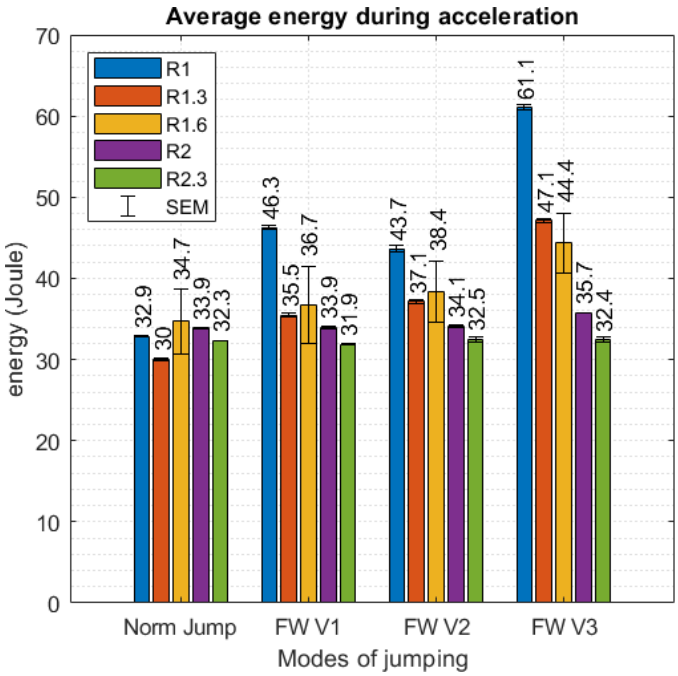

Fig. 10: The total mechanical energy delivered by the motor during acceleration per ratio, per jump averaged over 3 attempts.

5.5% and 0.4%. The percentage of field weakening during acceleration is also relatively low compared to other ratios with 38.1% and 11.2% relatively.

In table II an increase in height of 10% and 3.5% can be seen for respectively ratios 1.3 and 1.6 with an energy increase of respectively 56.9% and 27.9%. These are big energy increases compared to only a small increase in height. The last column of table II also shows this. For ratios 1.3

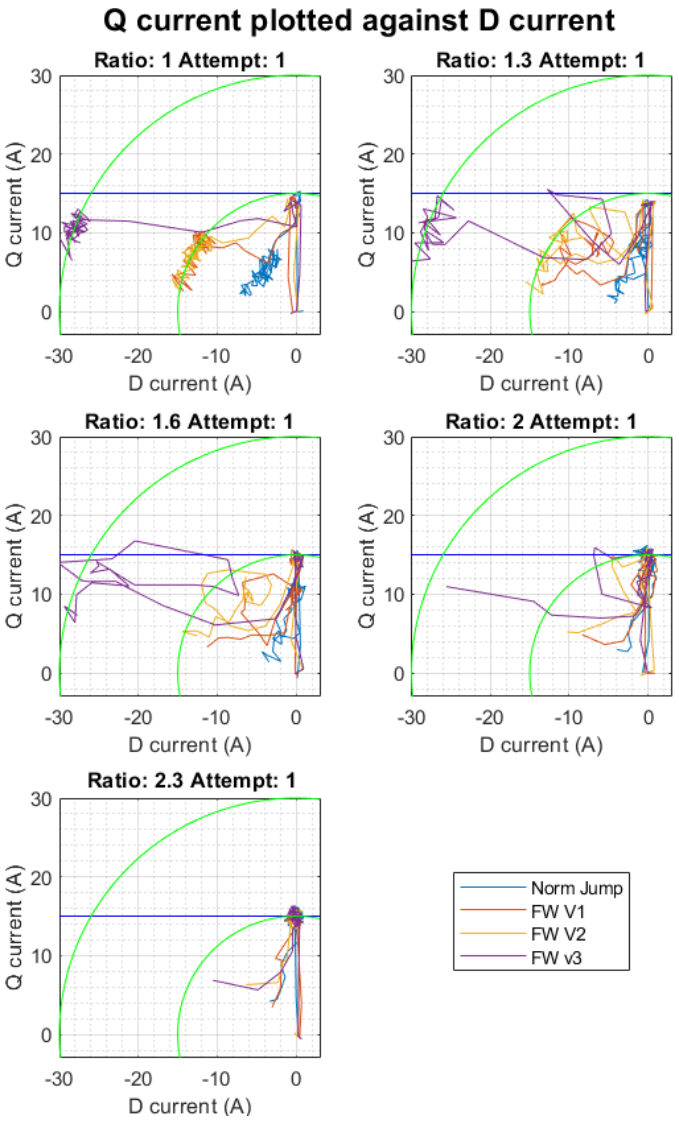

Fig. 11: The Quadrature axis current and the Direct axis current for all ratios for all modes for attempt 1. The inner and the outer green circle represent the a current limit of 15A and 30A. The horizontal blue line represents the quadrature axis current limit of 15A.

and 1.6, an increase of respectively 5.7% and 8% in energy is needed for an increase of 1% in height.

In table II an increase of 2.9% in height is noted for ratio 1. This is a gain in height and to accomplish this height, an energy increase of 85.8% was needed. This is a big energy increase compared to the increase in height. table II shows that for a 1% increase of height, an increase of 30% in energy occurred. The amount of samples field weakening was active during acceleration is almost equal for ratios 1 and 1.3 with 94.1% and 93.8%. The energy increase and height increase with ratios 1 and 1.3 is not almost equal.

A. *Height Increase*

In section V it can be seen that the increase in height is not the same as the increase in Energy. Where this energy ends up is uncertain. It can be dissipated into heat due to friction. A lot of friction during the assembly of the setup was found. The

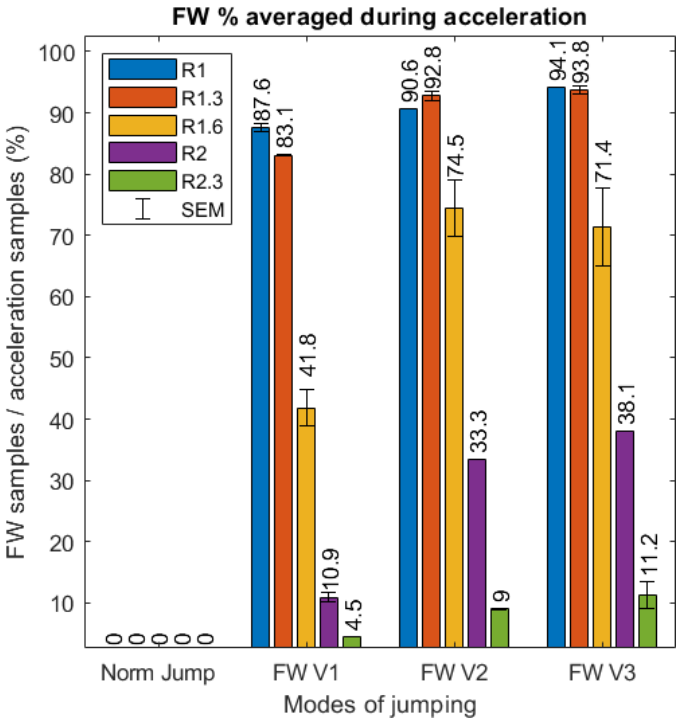

Fig. 12: percentage of field weakening used during acceleration per gearing ratio and averaged over the three attempts with the standard error of the mean (SEM).

Ratio	Height	Energy	FW Samples	Energy/Height
1	+2.9%	+85.8%	+94.1%	30
1.3	+10%	+56.9%	+93.8%	5.7
1.6	+3.5%	+27.9%	+71.4%	8.0
2	-2%	+5.5%	+38.1%	-2.6
2.3	-1.7%	+0.4%	+11.2%	-0.24

TABLE II: Per ratio the averaged percentages from 7,9 and 12 during FW V3, are displayed.

alignment of the poles had a lot of effect on the movement of the main body. The friction was also position-dependent. The setup also produced forces in the horizontal direction causing the linear bearings of the main body to be pushed vertically against the gliders.

The energy increase could also be dissipated by the mechanical brake mentioned in III-B3. It is difficult to calculate the kinetic energy and the potential energy of the setup during a jump due to the lack of height measurements during the jumps.

Almost the same FW sample percentage value of ratio 1 and 1.3 in section II means that during the acceleration only a short time of normal operation is persent before going into field weakening operation. This can be caused by the fact that a lower gear ratio (in normal operation mode) means a higher torque and thus a higher acceleration but a lower top velocity as was stated in table I meaning that the field weakening operating range is entered (too) earlier than a higher gear ratio. Or in other words, ratios 1 and 1.3 might be at the limit of the velocity they can reach and a higher gear ratio might be able to reach a higher velocity and jump height. This might mean that with a gearing ratio somewhere between 1.6 and 1.3 a higher jump height and a lower FW sample percentage can be found meaning that the field weakening operating range is entered later than with ratios 1 and 1.3.

Ratio 1.3 produces the highest absolute height and a higher maximum torque after the secondary gears than ratio 1.6, 2 and 2.3 according to table I. This means that with field weakening a higher torque can be produced without having a higher gear ratio which results in sacrificing maximum rotational velocity.

The energy per height column of I might even suggest that a lower energy per height value can be found somewhere between a ratio of 1 and 1.6 since 1.3 has the lowest energy to height ratio of the three ratios and this might not be the lowest value. However, the energy-to-height ratio might only say something about the efficiency of the applied energy, not about obtaining a higher jumping height. This might not result in an overall jumping height increment. This efficiency might be informative but not always leading since the effect might be more important than efficiency.

B. Current

The current not following the green circles in figure 11 and described in section IV-B does influence the performance of the field weakening modes. A reason for these dips in quadrature current might be that the voltage compensation for voltage losses discussed in section III-C3 was not enough. Another reason for this behavior might be a badly tuned current controller.

The reason that in figure 11 the currents for ratios 1, 1.3 and 1.6 reach the green circles indicates that field weakening algorithm is working and accomplishing some of the current commands. The current lines of ratios 2 and 2.3, not reaching the circles, indicates that the algorithm is not able to reach its field weakening current commands. This can also be seen in the phase plot of figure 8 where it is clear that due to the field weakening algorithm, the velocity is different along the movement for ratios 1, 1.3 and 1.6. For ratios 2 and 2.3 the phase plot is plotted on top of each other meaning that no variation is present in velocity meaning that the field weakening algorithm has no changing effect on the acceleration or velocity

C. Other Points of Concern

The errors that occurred during jumping might have an influence on the results. In section in table **??** an overview of these errors can be seen. For every gear ratio, the squatting position and the fully extended position were set via the control panel. This means that these positions, used by the program to accelerate from the squatting position to the fully extended position, might differ slightly between gearing ratios. The environment might also have changed since for example the motor temperature was not measured. The errors that occurred during testing might also add to the unreliability of the tests.

VI. Conclusion and Recommendations

A. Conclusion

Field weakening is used to successfully increase the jumping height of a jumping leg setup with 10.8% with an increase

of delivered mechanical energy of 56.9%. This is achieved without changing the drive train and only the gear ratio has been altered. An increase in height due to field weakening with this setup is dependent on the gearing ratio and thus on the maximum reachable velocity and the operating range of field weakening. Field weakening version 3 resulted in the highest height increase. The high increment in energy compared to the increment in height is not equal but the effect, for some applications, might be more important than efficiency. Using field weakening to increase the jumping height of a jumping leg setup, is suspected to have more potential than shown here when the mechanical energy is used more efficiently. With a different setup, these frictions can be tackled and less friction in the total setup can be achieved. With this new setup, a detailed model can be built and used to simulate the best gearing ratio for obtaining the highest height possible given that setup.

Field weakening can also be used to increase torque without sacrificing maximum rotational velocity which happens with introducing a lower gear ratio. This opens the door for using field weakening in robotic setups to increase jumping height but also have more torque available for other tasks without sacrificing maximum velocity.

The error rate that accompanies field weakening usage is a point of concern.

B. Recommendations

1) Energy Tracking: The tracking of the body height during the jumps with the same sample rate as the information like velocity, position and the currents from the motor controller, can be used to calculate the kinetic and potential energy. This way the amount of energy in the system can be calculated and the flow of the mechanical energy produced by the electric motor can be investigated.

2) DC Voltage Compensation: The DC voltage compensation can be applied better so that the current dips in the quadrature axis does not occur anymore. No current dips mean no torque dips.

3) Shielding of the System: The total system should be shielded with shielded cables and boxes around all components. During construction and pretesting, interference occurred in the wiring of the control panel when the motor controller was controlling the motor. Shielding should counter this interference. Interference in other signals can also be lower due to shielding. This might help with the reliability of the whole system.

4) Feedback Method: To counter the weaknesses of a model-based design, a feedback method can be integrated by upgrading the parameter estimation due to temperature. a Kalman filter-like design, combining the model-based and the feedback method, should be investigated to use the best of both worlds.

5) Friction: The friction, discussed earlier, obtained by the setup pushing the linear bearing perpendicular into the glider should be omitted since in a real robotic leg, this friction does not exist. The purpose of the gliders is to prevent the setup from falling and going straight up while minimizing friction to represent a jumping leg without gliders. The friction can be countered by omitting gliders by building a more realistic leg. The leg can then for instance be used in real robotic setups like is done in [4]. A solution like a fall screen can also be explored. The findings of [2] can be used to design the leg ratio for a more optimized jumper design. Due to this and the above mentioned, a complete redesign of the test platform is recommended.

6) Variable Gear Ratio: A variable gear system like the one presented in [4] in cooperation with the proposed field weakening strategy might have better performance than only the variable gear or only the field weakening solution. This should be investigated in the search for an explosive jumping robotic setup with better performance.

7) Demagnetization: The demagnetization prevention should be looked into in future work to prevent the magnets from demagnetizing. This could be of importance for using field weakening in the long-term setups.

REFERENCES

[1] P. M. Wensing, A. Wang, S. Seok, D. Otten, J. Lang, and S. Kim, "Proprioceptive actuator design in the MIT cheetah: Impact mitigation and high-bandwidth physical interaction for dynamic legged robots," *IEEE Transactions on Robotics*, vol. 33, pp. 509–522, 6 2017.

[2] E. W. Hawkes, C. Xiao, R. A. Peloquin, C. Keeley, M. R. Begley, M. T. Pope, and G. Niemeyer, "Engineered jumpers overcome biological limits via work multiplication," *Nature*, vol. 604, pp. 657–661, 4 2022.

[3] F. Meng, Q. Huang, Z. Yu, X. Chen, X. Fan, W. Zhang, and A. Ming, "Explosive Electric Actuator and Control for Legged Robots," *Engineering*, vol. 12, pp. 39–47, 5 2022.

[4] S. Morimoto, Y. Takeda, T. Hirasa, and K. Taniguchi, "Expansion of Operating Limits for Permanent Magnet Motor by Current Vector Control Considering Inverter Capacity," *IEEE Transactions on Industry Applications*, vol. 26, no. 5, pp. 866–871, 1990.

[5] W. Roozing, N. Kashiri, and N. G. Tsagarakis, "Enhanced Explosive Motion for Torque Controlled Actuators Through Field Weakening Control," in *IEEE International Conference on Intelligent Robots and Systems*, pp. 5972–5979, Institute of Electrical and Electronics Engineers Inc., 12 2018.

[6] S. P. . Sjoerd and . Rozendal, "FIELD-WEAKENING AND FATIGUE MANAGEMENT FOR EXPLOSIVE ROBOTICS," tech. rep.

[7] M. Mohammadnia, N. Kashiri, F. Braghin, and N. G. Tsagarakis, *Flux Regulation for Torque-controlled Robotics Actuators*. 2019.

[8] J. Ottosson and M. Alaküla, "A compact field weakening controller implementation," in *International Symposium on Power Electronics, Electrical Drives, Automation and Motion, 2006. SPEEDAM 2006*, vol. 2006, pp. 696–700, 2006.

[9] C. J. O'Rourke, M. M. Qasim, M. R. Overlin, and J. L. Kirtley, "A Geometric Interpretation of Reference Frames and Transformations: Dq0, Clarke, and Park," *IEEE Transactions on Energy Conversion*, vol. 34, pp. 2070–2083, 12 2019.

[10] C. Dufour, "Application note Park or DQ Transform variants Opal-RT Technologies Park/DQ transform variants 2 / 6," tech. rep., Opal-RT Technologies, 5 2018.

[11] J. Hendershot and T. Miller, *Design of Brushless Permanent-Magnet Motors*. 2010.

Ratio	Jump Mode	Attempt	Error
1	Norm Jump	1	Current limit violation
1	Norm Jump	2	Current limit violation
1	Norm Jump	3	Current limit violation
1.3	Norm Jump	1	Current limit violation
1.6	Norm Jump	3	Current limit violation
1.6	FW V3	1	Regen current violation
1.6	FW V3	2	Regen current violation
1.6	FW V3	3	Regen current violation
2.3	FW V3	2	Current or regen violation
2.3	FW V3	3	Current or regen violation

TABLE III: Errors reported by the motor controller during testing.

VII. Appendix

A. Errors During experiments

During the execution of these tests, the motor controller sometimes went into an error state meaning that the control was discontinued during these tests. In table I, the error states that occurred per ratio, jump mode and attempt can be seen. The bigger standard error of the mean bar for ratio 1.6 in figures 12, 10, 9,6 and 7 is the result attempt 3 from ratio 1.6. The power usage of the four different jumps was higher compared to attempt 1 or 2.